Molecular Spectroscopy Workbench

Effect of Dopants or Impurities on the Raman Spectrum of the Host Crystal

The disruption of crystalline symmetry by dopants or impurities in a crystal can affect the lattice vibrational modes of the host crystal. The manner in which the host-crystal Raman spectrum is affected is related to the site occupancy of the dopant or impurity. Not all bands are affected equally by the presence of heterogeneity in the crystal. Those Raman bands arising from lattice vibrational modes that involve a significant contribution of atomic motion from the substituted atom will manifest the most significant broadening or shifting of peak position. The purpose of this installment of "Molecular Spectroscopy Workbench" is to inform and educate users of Raman instrumentation about the effect of dopants or impurities on the Raman spectra of crystals. We do that here through a detailed discussion of the effects of dopants on the Raman spectra of $ZrGeO_4$ in the scheelite phase.

David Tuschel

Readers of "Molecular Spectroscopy Workbench" are aware that Raman spectroscopy is a convenient method for probing the chemical bonding and solid state structure of crystals. Moreover, it is sensitive to the presence of dopants, impurities, and crystal defects in the host-crystal lattice. The disruption of crystalline symmetry by dopants or impurities in a crystal can affect the lattice vibrational modes of the host crystal. If present at low concentrations (<1%), then the effect on the host lattice vibrational modes may not be perceptible. However, at levels greater than 1% dopants or impurities can be detected through the shifting and broadening of Raman bands of the host crystal. Moreover, new bands may appear that are absent in the Raman spectrum of the undoped or pure crystal. The manner in which the host-crystal Raman spectrum is affected is related to the site occupancy of the dopant or impurity. Therefore, one can infer from changes in the spectrum that dopants or impurities are present. Furthermore, the location of the dopants or impurities in the crystal lattice can be inferred from the particular bands affected. The purpose of this installment is to inform and educate users of Raman instrumentation about the effect of dopants or impurities on the Raman spectra of crystals. We do that here through a detailed discussion of the effects of dopants on the Raman spectra of $ZrGeO_4$.

$ZrGeO_4$ in the scheelite phase belongs to the C_{4h} crystal point group. Chains of 8-coordinate Zr^{4+} cations populate the *ab*-plane in the directions of the respective axes, whereas isolated GeO_4^{4-} tetrahedra alternate with the Zr^{4+} cations along the *c*-axis. A significant aspect of this structure is that

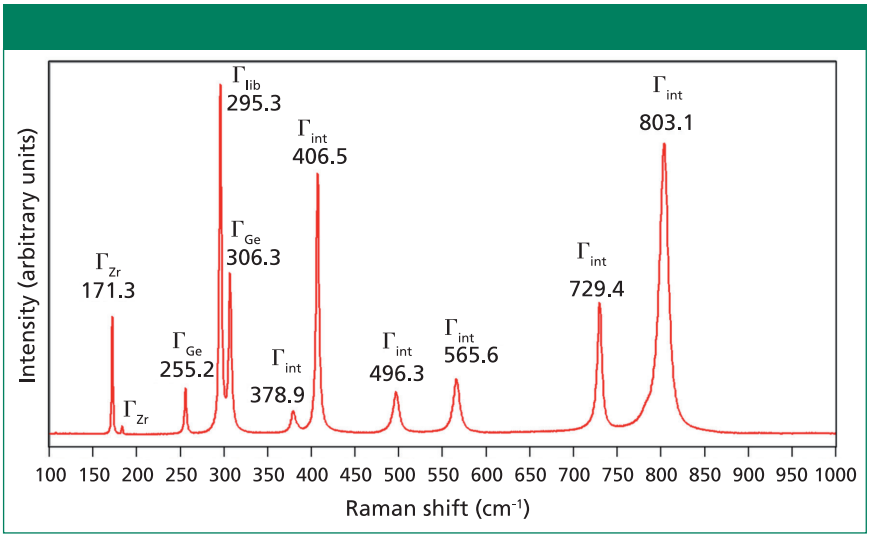

Figure 1: Raman spectrum obtained from a single crystal of $ZrGeO_4$.

the GeO_4^{4-} tetrahedra are distorted and exhibit compression along the *c*-axis. When activated by the presence of transition metal or lanthanide dopants, $HfGeO_4$ and $ZrGeO_4$ exhibit a broad blue luminescence when excited with X-rays. To understand the nature of the blue luminescence, studies have been performed to determine the local environment of the dopants (1). Specifically, there is a desire to know whether the dopant occupies the eightfold Zr^{4+} site or the fourfold GeO_4^{4-} tetrahedral coordination spheres.

The identification and assignment of those Raman bands most affected by the presence of transition metal or lanthanide dopants can be used to determine the site occupancy of the dopants. The first step is to assign the Raman bands to internal and external lattice vibrational modes. Here our distinction between internal and external modes pertains to the vibrational motions of the isolated GeO_4^{4-} tetrahedra. Those vibrational motions of the tetrahedra in which the center of mass does not move are regarded as *internal modes*. These modes approximate those of an isolated tetrahedron. In contrast, external modes are assigned to translational movement of the cation or tetrahedron or rotational motion of the tetrahedron as a whole. Regarding the rotational motions, external modes that involve the rotation of molecular groups about the center of mass are known as *librational modes*.

The irreducible representations of the optical phonons derived from a group theoretical treatment are

$$\Gamma_{optical} = 3A_g(R) + 5B_g(R) + 5E_g(R) + 4A_u(IR) + 3B_u(inactive) + 4E_u(IR) \quad [1]$$

where *IR*, *R*, and *inactive* represent infrared-active, Raman-active, and inactive modes, respectively. Furthermore, site-group analysis predicts the following external translational and librational modes:

$$\Gamma_{trans} = \Gamma_{Zr} + \Gamma_{Ge} = 2B_g(R) + 2E_g(R) + 2A_u(IR) + 2E_u(IR) \quad [2]$$

$$\Gamma_{lib} = A_g(R) + E_g(R) + B_u(inactive) + E_u(IR) \quad [3]$$

$$\Gamma_{ext} = \Gamma_{trans} + \Gamma_{lib} = A_g(R) + 2B_g(R) + 3E_g(R) + 2A_u(IR) + B_u(inactive) + 3E_u(IR) \quad [4]$$

The remaining internal modes can be attributed to the vibrational motions of the GeO_4 group:

$$\Gamma_{int} = \Gamma_{optical} - \Gamma_{ext} = 2A_g(R) + 3B_g(R) + 2E_g(R) + 3A_u(IR) + 2B_u(inactive) + 2E_u(IR) \quad [5]$$

The polarizability tensors for the Raman active modes are

$$A_g = \begin{pmatrix} a & 0 & 0 \\ 0 & a & 0 \\ 0 & 0 & b \end{pmatrix}, B_g = \begin{pmatrix} c & d & 0 \\ d & -c & 0 \\ 0 & 0 & 0 \end{pmatrix}, E_g = \begin{pmatrix} 0 & 0 & e \\ 0 & 0 & f \\ e & f & 0 \end{pmatrix}, \begin{pmatrix} 0 & 0 & -f \\ 0 & 0 & e \\ -f & -e & 0 \end{pmatrix} \quad [6]$$

A Raman spectrum from a single crystal of $ZrGeO_4$ is shown in Figure 1. This spectrum was obtained from one face of a single crystal, so the relative intensities of the bands will not be the same as those from another face of this same crystal or from a spectrum obtained from a powder sample of $ZrGeO_4$. That is an important consideration when comparing this spectrum of $ZrGeO_4$ with those obtained from other $ZrGeO_4$ crystals doped with other elements. Differences in the relative intensities of Raman bands between spectra from doped and undoped crystals are only meaningful when comparing spectra acquired from the same crystallographic faces with the same crystal orientation and incident laser polarization. The bands in the Raman spectrum of $ZrGeO_4$ shown in Figure 1 have been assigned to external translational, librational, and internal modes based on previous work (1–3). Only 11 of the 13 Raman active modes expected based on equation 1 are labeled in Figure 1 because not all of the bands are sufficiently strong in this particular crystal orientation.

Raman Spectroscopy of V- and Tb-Doped $ZrGeO_4$

Single crystals of $ZrGeO_4$ were prepared from a Li_2MoO_4•$2MoO_3$ flux containing 2 wt% ZrO_2 and fivefold excess of GeO_2. Dopants were added in the form of vanadium, terbium, or titanium oxides at various mole percentages (mol %) of the ZrO_2 value. Further details regarding crystal preparation can be found in a previous publication (1).

A Raman spectrum of vanadium-doped $ZrGeO_4$ along with that of undoped $ZrGeO_4$ for comparison are shown in Figure 2. The spectra were obtained from different crystallographic faces so differences in relative intensities of the spectra are expected. However, the differences in peak positions and band widths in the spectrum of the doped crystal can be attributed to disruption of the crystal lattice by the presence of V within the $ZrGeO_4$. We begin our analysis of the spectra by considering the bands that show little difference or a slight positive shift between the undoped and V-doped $ZrGeO_4$ at 171.8, 255.0, and 307.0 cm^{-1} ($ZrGeO_4$:V^{4+} peak positions). These bands are assigned to external modes of Zr and Ge motion, and the shifts of the bands because of the presence of V are +0.5, -0.2, and +0.7 cm^{-1}, respectively. Conversely, the bands at higher energy all shift to lower wavenumbers

and by more than 1 cm^{-1} as a result of the presence of V. In particular, note the -6.5 cm^{-1} shift from 295.3 cm^{-1} in the spectrum of pure $ZrGeO_4$ to 288.8 cm^{-1} in the V-doped spectrum. The directions and magnitudes of the changes in all band positions vary depending on the nature of the underlying lattice vibrational mode. In addition to the peak shifting, one can observe band broadening as a result of the doping. In particular, note how broad the 377.0 cm^{-1} band is in the V-doped spectrum compared to its counterpart at 378.9 cm^{-1} in the spectrum of $ZrGeO_4$. The 377.0 and 402.8 cm^{-1} bands are only partially resolved in the V-doped spectrum whereas their counterparts in the spectrum of undoped $ZrGeO_4$ are completely resolved. The disruption of long-range translational symmetry by the dopant at a crystal lattice site causes an increase in the distribution of phonon energy states and therefore a broadening of the Raman bands. Not all bands are affected equally by the presence of heterogeneity in the crystal. Those Raman bands arising from lattice vibrational modes that involve a significant contribution of atomic motion from the substituted atom will manifest the most significant broadening.

Doping $ZrGeO_4$ with terbium produces changes in the Raman spectrum similar to, but not as great in magnitude, as those observed in the spectrum of V-doped $ZrGeO_4$. A Raman spectrum of terbium-doped $ZrGeO_4$ along with that of undoped $ZrGeO_4$ for comparison are shown in Figure 3. You can see from the similar relative intensities of the bands of the spectra of doped crystals in Figures 2 and 3 that the Raman spectra were acquired from the same crystallographic faces of the V- and Tb-doped crystals. In general, the bands shift and broaden with Tb doping just as observed for V doping. However, the changes in the spectrum of Tb-doped $ZrGeO_4$ are not as great as those observed for V-doped $ZrGeO_4$. In particular, the 378.5 cm^{-1} peak in the Tb-doped $ZrGeO_4$ spectrum is not as broad as its counterpart at 377.0 cm^{-1} in the V-doped $ZrGeO_4$ spectrum. The dopant levels are similar in these two

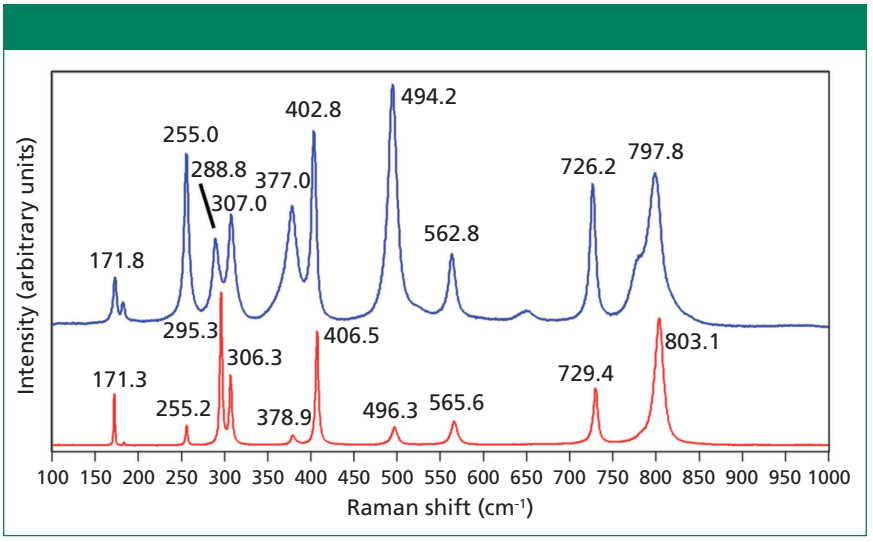

Figure 2: Raman spectra of single crystals of $ZrGeO_4$ (red) and $ZrGeO_4$ doped with V (blue).

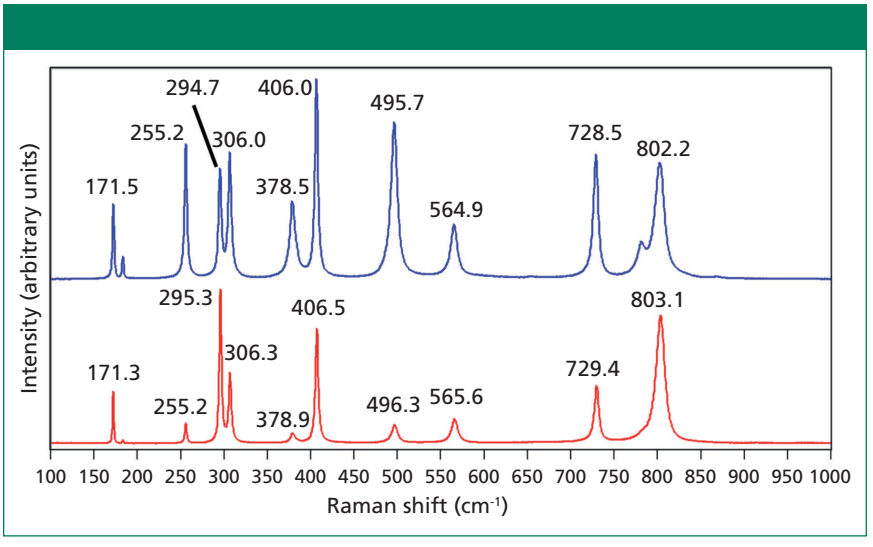

Figure 3: Raman spectra of single crystals of $ZrGeO_4$ (red) and $ZrGeO_4$ doped with Tb (blue).

crystals, so we might expect the effects on the $ZrGeO_4$ Raman spectrum to be similar as well. However, the effects of V doping are clearly greater than those from Tb. Why is that? To help us answer that question, we examine the effects of a third dopant, titanium, on the Raman spectrum of $ZrGeO_4$. Titanium is a transition metal immediately following vanadium in the periodic table of elements, whereas terbium is a lanthanide. We expect the chemical bonding of the transition metal dopants to the surrounding atoms to be different from that of the lanthanide.

Raman Spectroscopy of Titanium-Doped $ZrGeO_4$

Crystals were prepared with various degrees of titanium doping. One such crystal reveals through X-ray diffraction a lattice parameter change corresponding to a 10% to 15% incorporation of Ti into the $ZrGeO_4$ lattice. A Raman spectrum of the 10–15% titanium-doped $ZrGeO_4$ along with that of undoped $ZrGeO_4$ for comparison is shown in Figure 4. The shifts and broadening of the $ZrGeO_4$:Ti^{4+} Raman bands relative to those in undoped $ZrGeO_4$ are significant and comparable to those in the spectrum of $ZrGeO_4$:V^{4+} shown in Figure 2. The most significant shifts occur for the bands at ($ZrGeO_4$ peak positions) 295.3, 378.9, 406.5, and 565.6 cm^{-1} to 286.2, 374.1, 401.3, and 559.8 cm^{-1} in the $ZrGeO_4$:Ti^{4+} spectrum, re-

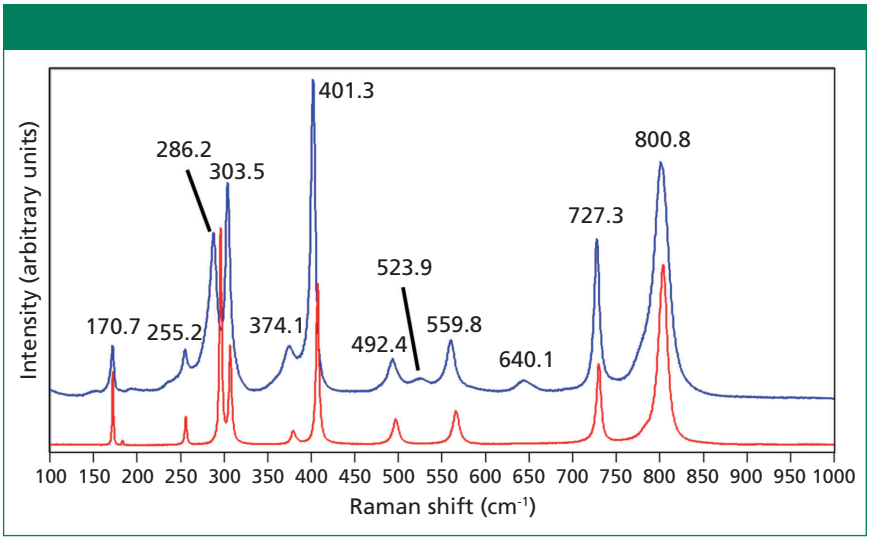

Figure 4: Raman spectra of single crystals of $ZrGeO_4$ (red) and $ZrGeO_4$ doped with Ti (blue).

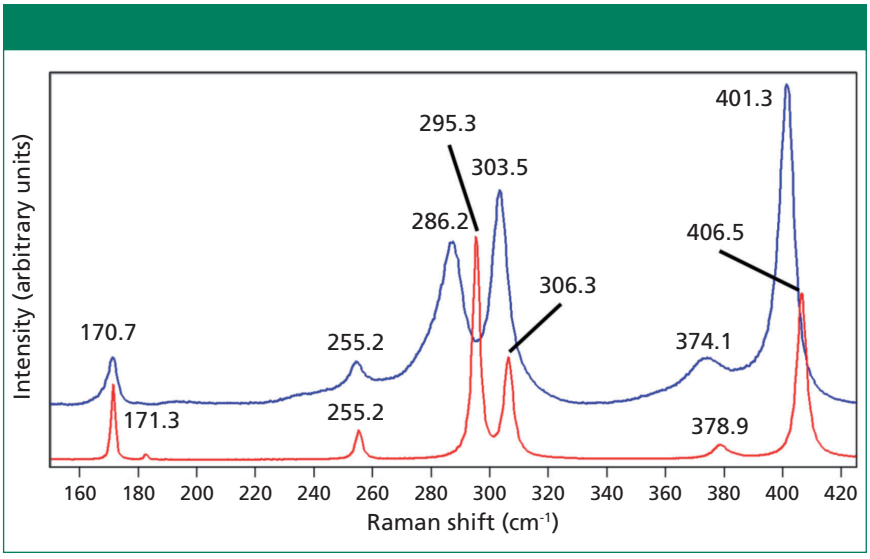

Figure 5: Raman spectra of single crystals of $ZrGeO_4$ (red) and $ZrGeO_4$ doped with Ti (blue). Ti occupancy of the Ge site causes Raman bands to shift and broaden relative to those in undoped $ZrGeO_4$.

spectively. Also, a band emerges at 640.1 cm^{-1} with Ti doping that is not present in the spectrum of pure $ZrGeO_4$. That portion of the spectrum between 150 and 425 cm^{-1} has been expanded in Figure 5 so that you can clearly see the significant changes to several of the bands. The Raman bands most affected by Ti doping are shown along with their mode assignments in Table I. Similar to our observations with V doping, we see that the low energy modes at 171.3 and 255.2 cm^{-1} ($ZrGeO_4$ peak positions) are weakly or not affected at all by Ti doping. That only some of the bands shift as a result of Ti doping suggests that Ti is not indiscriminately positioned, but rather preferentially occupies specific lattice sites. The fact that the bands most affected by Ti doping are all assigned to lattice vibrational modes involving GeO_4 motion indicates that the Ge position is the site of occupancy.

To further characterize the effect of Ti doping on the Raman bands of the host lattice $ZrGeO_4$, we make use of what I have previously called *Raman crystallography* (5). Raman crystallography can be used for the characterization of the atomic structure of solids because Raman scattering depends on the polarization and direction of the incident laser light, the crystal symmetry and orientation of the solid sample, and the direction and polarization of the collected Raman scattered light. The Raman polarizability tensor is fixed relative to the positions of the atoms and the directions of the bonds between them. Therefore, for a crystal fixed in space the Raman signal is dependent on the crystal symmetry and orientation of the sample relative to the direction and polarization of the incident and collected light. The expression for Raman scattering intensity used in the application of Raman crystallography is

$$I_R = I_L K \left| \bar{E}_i \bullet \alpha' \bullet \bar{E}_s \right|^2 \Omega \qquad [7]$$

where I_R is the Raman scattering intensity, I_L is the intensity of the incident laser light, K is a factor incorporating the dependence on the frequency of the incident laser light and the standard cross section, E_i the polarization of the incident light, and E_s and Ω are the polarization and solid angle, respectively, at which scattered light is collected. The significance of this expression for work with crystals is that Raman scattering intensity is proportional to the square of the dot product of the incident electric field vector, Raman polarizability tensor, and scattering vector. It is of great importance that the forms (whether elements are zero or nonzero) of the polarizability tensors for crystals are dictated by the symmetry point groups of the crystal class to which the material belongs. The absolute magnitude of the tensor elements is dictated by the specific chemical bonds between the atoms. However, whether a tensor element is zero or nonzero is entirely dictated by the crystal symmetry. The forms of the Raman tensor are the same for all lattice vibrational modes of the same symmetry species. Therefore, the normalized Raman signal strength as a function of crystal orientation should be the same for all Raman bands assigned to vibrational modes of the same symmetry species.

The experimental arrangement for Raman crystallography used a 100× microscope objective to focus a 532-nm laser beam incident upon the <001> face of the $ZrGeO_4$ crystal

Table I: Mode assignment of $ZrGeO_4$ bands most affected by Ti doping

Peak Position (cm^{-1})	Mode Assignment
295.3	Γ_{lib} (GeO_4)
378.9	Γ_{int} (GeO_4)
406.5	Γ_{int} (GeO_4)
565.6	Γ_{int} (GeO_4)

doped with Ti. Backscattered light was collected in two configurations with the analyzer either parallel or perpendicular with respect to the incident polarization. Spectra were then acquired in 5° rotational increments as the crystal was rotated about the axis normal to the <001> crystal face. The Raman responses from this measurement of two B_g modes at 171 and 727 cm^{-1} and with the Raman analyzer oriented perpendicular to the incident laser polarization are shown in Figure 6. The variations of signal strength with crystal orientation are the same for the 171 and 727 cm^{-1} bands as we would expect for two bands of the same symmetry species. Note that these two bands are among those that manifest little change in their position or width as a result of Ti doping. However, as you can see in Figure 5, the 401 cm^{-1} band in the Ti-doped $ZrGeO_4$ spectrum is significantly shifted relative to its counterpart in the undoped $ZrGeO_4$ spectrum. This band too belongs to the B_g symmetry species. The Raman responses from this measurement of two B_g modes at 401 and 727 cm^{-1} and with the Raman analyzer oriented perpendicular to the incident laser polarization are shown in Figure 7. Here we have again plotted the response of two bands of the same symmetry species, but the Raman crystallographic responses are no longer in phase. We note that the 401 cm^{-1} band has been significantly affected by Ti doping as manifested in its shift to a lower wavenumber. The plots of these two B_g Raman responses as a function of crystal orientation are no longer in phase because of the disruption of the crystal lattice symmetry by the presence of the Ti dopant and its effect on the B_g mode at 401 cm^{-1}.

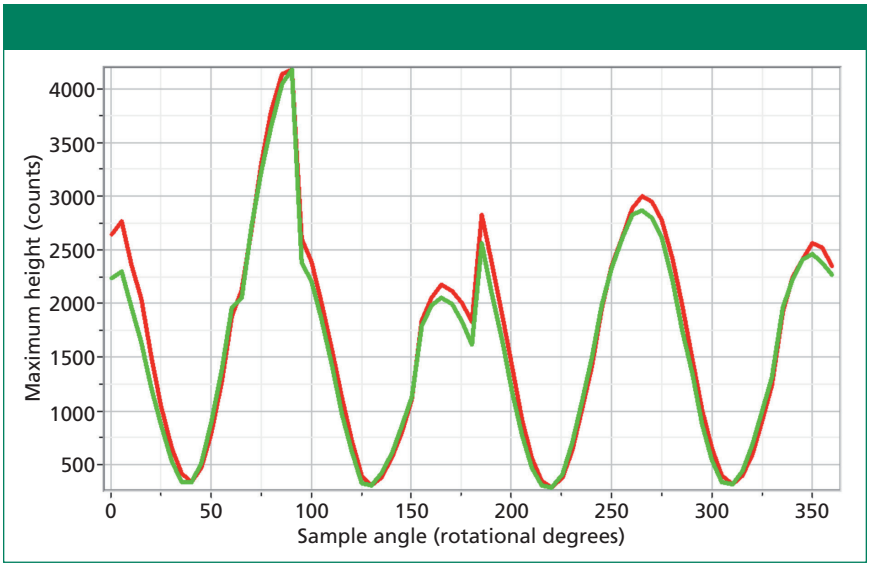

Figure 6: Raman signal strength of 171 cm^{-1} (green) and 727 cm^{-1} (red) bands of the Ti-doped $ZrGeO_4$ <001> crystal face as a function of crystal orientation in the <001> plane and with the Raman analyzer oriented perpendicular to the incident laser polarization. Both bands belong to the B_g symmetry species.

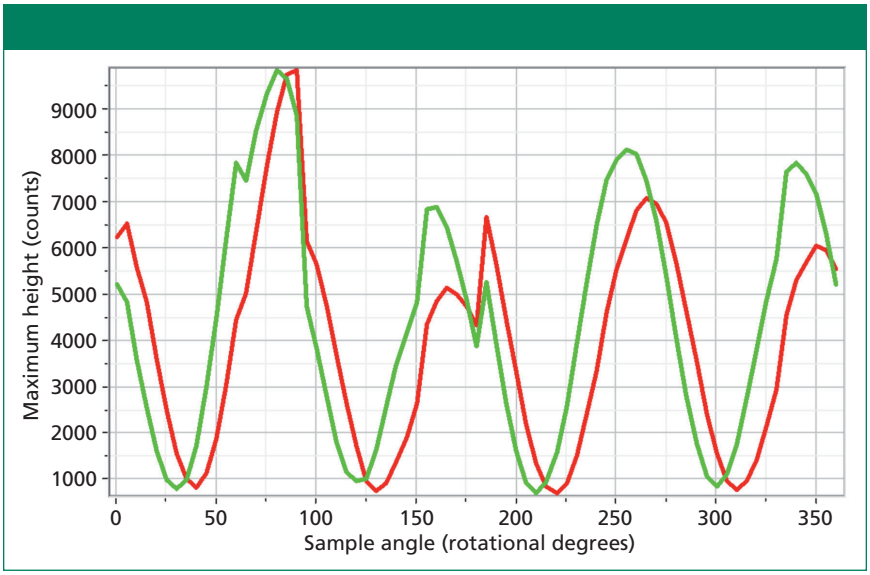

Figure 7: Raman signal strength of 401 cm^{-1} (green) and 727 cm^{-1} (red) bands of the Ti-doped $ZrGeO_4$ <001> crystal face as a function of crystal orientation in the <001> plane and with the Raman analyzer oriented perpendicular to the incident laser polarization. Both bands belong to the B_g symmetry species.

Chemical Bonding and the Doping of $ZrGeO_4$

Here we elaborate on the band structure analysis and offer an explanation for the effects of Ti doping on the Raman spectrum of $ZrGeO_4$. The affected bands have two common characteristics. Specifically, their Raman tensors have nonzero α_{xx} and α_{xy} tensor elements and that they can be assigned to GeO_4 rotation or Ge-O bending motions within the *ab*-plane. The Γ_{lib} mode in Table I is a GeO_4 rotation. We assign the Γ_{int} bands in Table I to Ge-O bending motions based on the application of the site group method to correlate the S_4 site symmetry species to an XY_4 free molecule of T_d symmetry. The correlation diagram for the GeO_4^{4-} group in the $ZrGeO_4$ crystal is shown in Figure 8.

The free GeO_4^{4-} group with T_d symmetry has four normal vibrational modes consisting of A_1 (υ_α) symmetric

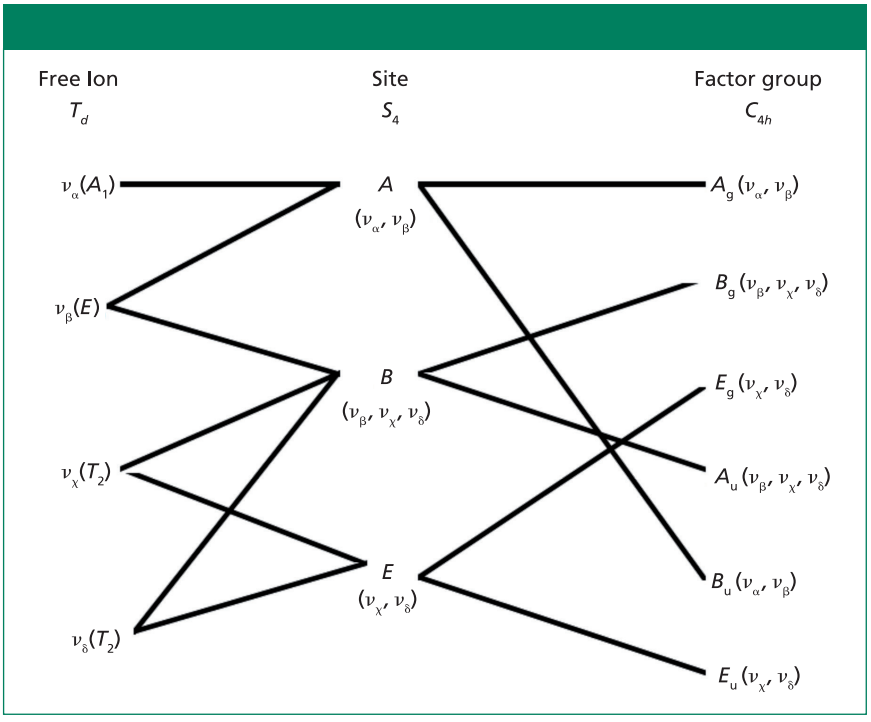

Figure 8: Correlation diagram for the GeO_4^{4-} group in the $ZrGeO_4$ crystal.

Table II: Correlation of the GeO_4^{4-} internal modes with T_d free ion

Normal vibration	T_d - free ion	C_{4h} - crystal
Symmetric stretch	$A_1(\nu_\alpha)$	$A_g(\nu_\alpha) + B_u(\nu_\alpha)$
Symmetric bend	$E(\nu_\beta)$	$A_g(\nu_\beta) + B_u(\nu_\beta)$ $B_g(\nu_\beta) + A_u(\nu_\beta)$
Antisymmetric stretch	$T_2(\nu_\chi)$	$B_g(\nu_\chi) + A_u(\nu_\chi)$ $E_g(\nu_\chi) + E_u(\nu_\chi)$
Antisymmetric bend	$T_2(\nu_\delta)$	$B_g(\nu_\delta) + A_u(\nu_\delta)$ $E_g(\nu_\delta) + E_u(\nu_\delta)$

stretch, E (υ_β) symmetric bend, T_2 (υ_χ) antisymmetric stretch, and T_2 (υ_δ) antisymmetric bend. The symmetry of the free GeO_4^{4-} group is lowered to S_4 in the crystal, and the free ion T_d modes can be correlated to the internal modes of the factor group C_{4h} $ZrGeO_4$ crystal. That correlation of the Td local vibrational modes to C_{4h} phonons is shown in Table II.

Regarding our assignment and correlation of $ZrGeO_4$ bands to local Td modes, we expect the stretching modes to constitute the highest energy phonons in the spectrum, and based on our previous work the bands at 729.4 (B_g), 782 (E_g) (shoulder), and 803.1 cm^{-1} (A_g) have the appropriate symmetries to correlate to υ_χ (B_g), υ_χ (E_g) and υ_α (A_g), respectively (1). The remaining Γ_{int} bands are at 378.9 (A_g), 406.5 (B_g), 496.3 (E_g), and 565.6 cm^{-1} (B_g), which by symmetry correlate to υ_β (A_g), υ_β (B_g), υ_δ (E_g) and υ_δ (B_g), respectively. Of those four Γ_{int} bands, the A_g and B_g modes are among those most affected by Ti doping. Indeed, the bands listed in Table I as those most affected by Ti doping constitute the entire set of combined A_g and B_g bending and rotational modes for $ZrGeO_4$. There is one E_g bending mode and one E_g rotational mode, both of which are not as strongly affected by Ti doping. Note, however, that the nonzero E_g tensor elements are α_{xz}, α_{zx}, α_{yz}, and α_{zy}. In contrast, the strongly affected A_g and B_g modes have nonzero α_{xx}, α_{yy}, or α_{xy} (α_{yx}) tensor elements. Therefore, we conclude that Ti^{4+} substitution for Ge^{4+} significantly affects Raman bands arising from rotational and bending motions of the GeO_4^{4-} group about the *c*-axis, within the *ab*-plane.

Here we offer an explanation in terms of chemical bonding for the effects of Ti doping on the Raman spectra of $ZrGeO_4$. The tetrahedral GeO_4^{4-} group is formed by a combination of the oxygen orbitals and sp^3 hybridized atomic orbitals from Ge^{4+}. However, if Ti^{4+} is substituted for Ge^{4+}, the atomic orbitals of the central atom are no longer sp^3 hybridized. The 4s (a_1), 4p (t_2), 3d (e), and 3d (t_2) atomic orbitals of Ti^{4+} will, in a tetrahedral coordination, transform to the molecular orbitals a_1, t_2, e, and t_2, respectively. One a_1 and three t_2 molecular orbitals form σ-bonding orbitals in the tetrahedral structure. In particular, note that the t_2 bonding orbitals are formed by a hybridization of Ti^{4+} d (t_2) and p (t_2) orbitals. The 3d (e) atomic orbitals would transform to e nonbonding molecular orbitals. However, metal oxides readily form π bonds, and the 3d (e) orbitals can form π-bonding orbitals with the ligand in a tetrahedral structure. If π bonding does occur, then the local electronic structure of the TiO_4^{4-} tetrahedron is significantly different from that of the sp^3 hybridized GeO_4^{4-} tetrahedron. In particular, we could expect the $d_{x^2-y^2}$ (e) orbital involved in π bonding to hinder rotation of TiO_4^{4-} in the *ab*-plane, thereby damping lattice vibrational modes related to the unhindered rotation of the sp^3-hybridized GeO_4^{4-} tetrahedron. Consequently, Raman bands arising from GeO_4^{4-} rotations should shift and perhaps broaden to a lower wavenumber, which is what we observe.

The explanation and chemical interpretation regarding the chemical bonding of Ti^{4+} with surrounding oxygen atoms applies equally well to V^{4+} in Ge site occupancy. The transition metal dopants have a far greater effect on the lattice spectrum of $ZrGeO_4$ than does the lanthanide Tb dopant because of the role their d-orbitals play in chemical bonding to the crystal lattice.

Conclusion

The disruption of crystalline symmetry by dopants or impurities in a crystal can affect the lattice vibrational modes of the host crystal. The manner in which the host-crystal Raman spectrum is affected is related to the site occupancy of the dopant or impurity. Not all bands will be affected equally by the presence of heterogeneity in the crystal. Those Raman bands arising from lattice vibrational modes that involve a significant contribution of atomic motion from the substituted atom will manifest the most significant broadening or shifting of peak position. Raman spectroscopy has been used to characterize the effects of doping $ZrGeO_4$ with V, Ti, and Tb. We find that whereas all of the modes most affected by Tb, Ti, or V doping are those arising from the GeO_4^{4-} group, not all of the GeO_4^{4-} modes are strongly affected by doping. Substitution of either Ti^{4+} or V^{4+} for Ge^{4+} significantly affects Raman bands arising from the rotational and bending motions of the GeO_4^{4-} group about the *c*-axis, within the *ab*-plane. We propose an explanation for the effects by the transition metals based on group and molecular orbital theory.

Acknowledgment

The crystals were prepared by Dr. Pat Lambert of Transparent Materials in Rochester, New York.

References

(1) D.D. Tuschel and P.M. Lambert, *Chem. Mater.* **9,** 2852–2860 (1997).
(2) D. Michel, M.T. Van Den Borre, and A. Ennaciri, *Adv. Ceram.* **24A** (*Sci. Technol. Zirconia* 3), 555–562 (1988).
(3) M.T. Vandenborre, D. Michel, and A. Ennaciri, *Spectrochim. Acta A* **45A,** 721–727 (1989).
(4) G. Turrell in *Practical Raman Spectroscopy*, D.J. Gardiner and P.R. Graves, Eds. (Springer-Verlag, Berlin, 1989), chap. 2, pp. 13–54.
(5) D. Tuschel, *Spectroscopy* **27**(3), 22–27 (2012).

David Tuschel is a Raman applications manager at Horiba Scientific, in Edison, New Jersey, where he works with Fran Adar. David is sharing authorship of this column with Fran. He can be reached at: SpectroscopyEdit@UBM.com

For more information on this topic, please visit: www.spectroscopyonline.com